Superconducting Long-Range Proximity Effect through the Atomically Flat Interface of a Bi 2 Te 3 Topological Insulator

Vasily S Stolyarov, Stephane Pons, Sergio Vlaic, Sergey V Remizov, Dmitriy Shapiro, Christophe Brun, Sergey I Bozhko, Tristan Cren, Tatiana V Menshchikova, Evgueni Chulkov, et al.

Superconducting Long-range Proximity Effect Through The Atomically Flat interface of Bi_2Te_3 Topological Insulator

Vasily S. Stolyarov,[*,†,‡,¶] Stephane Pons,[§] Sergio Vlaic,[§] Sergey V. Remizov,[¶] Dmitry S. Shapiro,[¶] Christophe Brun,[‖] Sergey I. Bozhko,[⊥] Tristan Cren,[‖] Tatiana V. Menshchikova,[#] Evgeny V. Chulkov,[#,@,△] Walter V. Pogosov,[¶] Yuriy E. Lozovik,[▽,¶,††] and Dimitri Roditchev[§]

†*Laboratoire de Physique et d'Etudes des Materiaux, ESPCI-Paris, CNRS and UPMC Univ Paris 6, 75005 Paris, France*
‡*TQPSS Lab, Center for Photonics and 2D Materials, Moscow Institute of Physics and Technology, Dolgoprudny, 141700 Moscow, Russia*
¶*Dukhov Research Institute of Automatics (VNIIA), Moscow 127055, Russia*
§*Laboratoire de Physique et d'Etudes des Materiaux, ESPCI-Paris, CNRS and UPMC Univ Paris 6 - UMR 8213, 75005 Paris, France*
‖*Institut des Nanosciences de Paris, Sorbonne Universites, UPMC Univ Paris 6 and CNRS-UMR 7588, F-75005 Paris, France*
⊥*Institute of Solid State Physics RAS, 142432 Chernogolovka, Russia*
#*Tomsk State University, 634050 Tomsk, Russia*
@*St. Petersburg State University, 198504 St. Petersburg, Russia*
△*Departamento de Fisica de materiales, Facultad de Ciencias Quimicas, UPV/EHU and Centro de Fisica de Materiales, Centro Mixto CSIC-UPV/EHU, Apartado 1072, 20080 San Sebastian/Donostia, Basque Country, Spain*
▽*Institute of spectroscopy RAS 108840 Troitsk, Moscow, Russia*
††*MIEM at National Research University – Higher School of Economics, Moscow*

E-mail: vasiliy.stoliarov@gmail.com

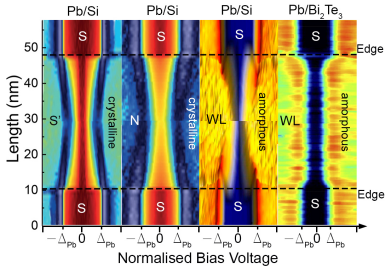

Abstract

We report on structural and electronic properties of superconducting nano-hybrids made of Pb grown in the ultrahigh vacuum on the atomically clean surface of single crystals of topological Bi_2Te_3. In-situ Scanning Tunneling Microscopy and Spectroscopy demonstrated that the resulting network is composed of Pb-nanoislands dispersed on the surface and linked together by an amorphous atomic layer of Pb, which wets Bi_2Te_3. As a result, the superconducting state of the system is characterized by a thickness-dependent superconducting gap of Pb-islands and by a very unusual position-independent proximity gap between them. Furthermore, the data analysis and DFT calcu-

lations demonstrate that the Pb-wetting layer leads to significant modifications of both topological and trivial electronic states of Bi_2Te_3, which are responsible for the observed long-range proximity effect.

Studies of structural and electronic phenomena occurring at the interfaces of two contacting materials are among the most appealing research fields in physics and nanotechnology. By putting two materials together, one can induce at their interface novel electronic properties absent in one or both materials. Famous examples are the formation of a two-dimensional electron gas at the interface between two semiconductors,[1] superconductivity appearing at the interface between two insulators, $LaAlO_3$ and $SrTiO_3$,[2] or angle-tuned electronic properties of bi-layer graphene,[3] to cite a few.[4–11] Another possibility is the extension of the desired properties into a given material from a "source" material by *proximity*. In this way, the superconductivity can be induced in normal metals[12–19] or even in semiconductors,[20–23] but also a magnetism[24] or an enhanced spin-orbit coupling.[25–28]

In this respect, the interface between superconductors (S) and a topological insulator (TI) is expected to induce by proximity peculiar properties such as unconventional superconductivity.[20,25] Topologically protected surface states[29–37] are not only attractive from the fundamental point of view, such as the realization of Majorana modes,[38–40] but also for spintronics applications, in the view of their robustness and the forbidden backscattering.[41–43] The couple Pb/Bi_2Te_3 is a good candidate for such a study. Bi_2Te_3 is a three-dimensional (3D) TI showing high electron mobility of topological (surface) states and a relatively low contribution of trivial (bulk) electronic states to the total electron transport .[28] Single crystals of Bi_2Te_3 are available, and the atomically clean surface of the material can be prepared in a vacuum by mechanical cleavage. On the other side, Pb is a good candidate to complete the interface since it is a well-known conventional s-wave superconductor with accessible critical temperature T_C^{bulk}=7.2 K. Pb remains superconducting in very thin films down to a few atomic

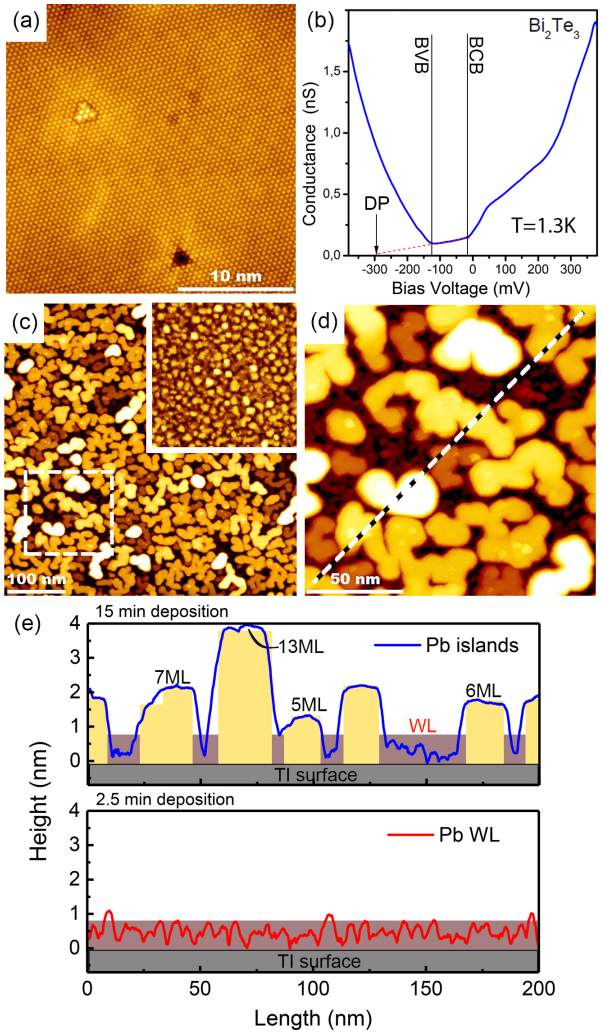

Figure 1: Structure of studied Pb/Bi_2Te_3 hybrids. STM data acquired at 1.3 K: (a) – $30 \times 30 nm^2$ STM image of UHV cleaved Bi_2Te_3 surface obtained before Pb islands deposition; (b) – Averaged STS dI/dV(V) spectra of atomically clean Bi_2Te_3 surface obtained (red dashed line is linear extrapolation for Dirac point (DP) and vertical black lines determine the value of BVB and BCB energies); (c) – $300 \times 300 nm^2$ STM image of Pb islands on the surface of Bi_2Te_3 after 15 minute of Pb deposition. The Insert depict $100 \times 100\ nm^2$ wetting layer (after 2.5 min of lead deposition). (d) – $140 \times 140 nm^2$ STM image of Pb islands - zoom from white dashed square (c); (e) – profile along dashed line cross-section depicted on figure (d) (top panel, blue line) and typical wetting layer roughness on the same scale (bottom panel, red line) taken after 2.5 min of lead deposition (c(insert))

layers,[44–46] and in the form of ultra-small 3D nanostructures, reaching the Anderson limit.[47] Transport measurements of Pb/Bi_2Te_3 hybrid structures revealed the existence of a strong superconducting proximity effect in both c- and a, b- crystallographic directions of Bi_2Te_3.[20] Recent sensitive experiments showed that the superconductivity induced in TI surface layer can be ballistic[23] or even unconventional[25] and consistent with the order parameter having $p_x + ip_y$ component.

In this work, we report on local properties of Pb/Bi_2Te_3 hybrids composed of few-nanometer thick superconducting nano-islands of Pb dispersed on the atomically clean surface of Bi_2Te_3; the latter is wet by an atomically thin amorphous layer of Pb (WL). The local insight is brought by Scanning Tunneling Microscopy and Spectroscopy (STM/STS), providing precious information about local superconducting properties and their spatial evolution, as compared to previously reported global transport properties.[20,25] We found that expectedly, the superconducting gap of Pb-nano-islands depends on their thickness.[44] In contrast, the proximity induced gap in the amorphous-Pb-wetting layer on top of Bi_2Te_3 is robust and almost independent of the distance to the islands. This is not typical for the diffusive proximity regime; it is also at variance with most of previous reports on Pb-coupled systems such as Pb/HOPG,[48] Pb/InAs,[49] Pb/amorphous-Pb[46] Pb/Sb(111)[50] and Pb/graphene[22] in which a rapid decay of superconducting correlations inside the proximity regions was observed. Moreover, in our case, the characteristic energy scale of the proximity induced gap, $\Delta_{WL}^{amorph} \sim 0.55$ meV$\approx 0.5\Delta_{Pb}$ (Δ_{Pb}^{bulk}(3K)=1.23 meV, (T_c^{bulk}=6.2 K)),[44] witnesses a powerful proximity effect between the superconducting islands, well consistent with the results of macroscopic measurements[20] and does not correspond to the previously presented results in Ref.[45] where native superconducting gap Δ_{WL}^{cryst} =0.23 meV (crystalline WL T_c=1.8 K) was observed.

By considering the numerically simulated detailed electronic structure of the studied system, we point out that the precise mechanism of superconducting proximity is much more subtle than a direct "spreading" of superconducting correlations to the topologically protected surface state of TI. Even one monolayer of Pb dramatically (ML_{Pb}=0.286 nm) modifies the electronic structure of Bi_2Te_3, leading to a downward band bending[51] and, possibly, forming the 2D accumulation layer of the bulk electrons. The detailed picture depends on the number of atomic layers of Pb present on the surface of Bi_2Te_3.

Figure 1 provides a summary of the structural properties of studied samples. The topographic STM image in Fig. 1(a) obtained after in-vacuum Bi_2Te_3 cleavage reveals the atomically clean surface on which typical structural defects[52–54] are observed. A typical $dI(V)/dV$ spectrum measured at the Bi_2Te_3 surface in a large energy window around the Fermi level is presented in Fig.1(b); the position of the Dirac point (DP), the top of the valence band (BVB) and the bottom of the conduction band (BCB) are indicated. Fig. 1(c) presents the STM image of the sample 15 minutes after the deposition of Pb. The Pb-islands form a non-connecting network. Fig. 1(d) is a zoom in on the studied area (in Fig. 1(c) it is indicated by a white square). The islands have a flat top and different heights 1-4 nm (3-13 atomic layers of Pb). The typical lateral size of Pb-islands is 30-40 nm.

Dark areas between the islands are amorphous Pb-wetting regions of Bi_2Te_3. We expect that the Pb layer under the Pb island is recrystallized thus forming atomically flat lower interface as it was already shown for Pb/Si(111) where an amorphous wetting layer exits between crystallized islands.[55] Fig. 1(e)(top panel, blue line) is the profile taken along the white dashed line presented in Fig. 1(d) and (bottom panel, red line) a cross-section taken somewhere on the surface shown in Fig. 1(c(insert)), which correspond to 2.5 min of Pb deposition when we observe just WL. The coloured background reflects the thickness of the amorphous WL (brawn) and the height of individual single-crystal islands (yellow), where 0 corresponds to the atomically smooth surface of the TI.

Figure 2 deals with the spatial distribution of electronic properties of objects under study.

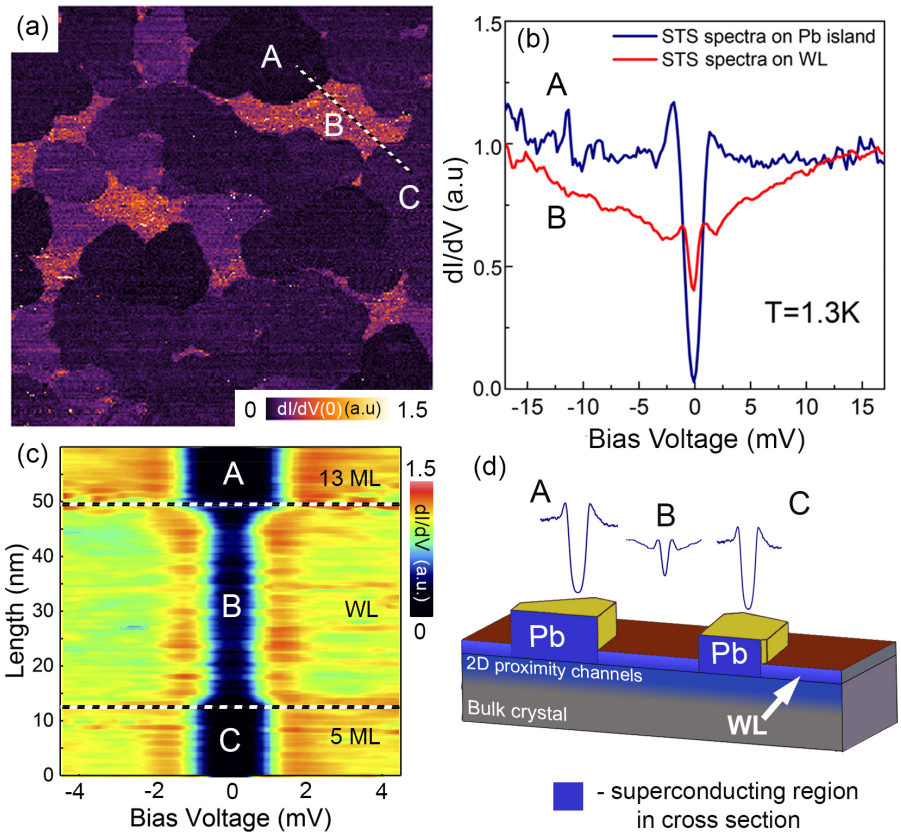

Figure 2: STS data acquired at 1.3 K. (a) – zero bias conductance map of the same areal as Fig.1(d); (b) – dI/dV(V) spectrum spatial evolution between Pb island (A) and Pb-wetting layer (B) deposited on atomically flat surface of Bi_2Te_3; (c) – average spectrum of Pb islands (A, C) and on top of the Pb-wetting layer (B); (d) – 3D schematic depiction of the proximity effect distribution at Pb/Bi_2Te_3/Pb-wetting layer interface.

Fig. 2(a) shows zero bias conductivity of different regions, provided Pb islands are already formed on the surface after 15 minutes of deposition (Fig. 1(d)). In this case, a pronounced superconducting gap is open both in the islands (A,C) and in the wetting layer (B). Fig. 2(b) shows experimentally measured spatial evolution of dI/dV spectrum along the normal direction to the edge of the island (A) and wetting layer (B) (Fig. 2(a)). It is seen that the superconducting gap in WL drops on the short length scale of the order of a nanometer and then stays essentially constant through the whole WL area between islands. This behaviour is similar to the one reported in Ref.[45] for Si substrate, but the length scale for the spatial evolution of the gap in the present case is much shorter. In our system gap drops by the factor close to two, while in Ref.[45] it drops by the factor of nearly four. Typical spectra on Pb island and WL are shown in Fig. 2(c). It should be noted that a typical gapless spectrum of an amorphous WL of lead far from the island was studied in Ref.[46] The amorphous-WL/Si system has the Coulomb blockade effect, similar to what we observe in our TI based system; it indicates the presence of tunnelling junctions between disordered conductors.[56] The whole scenario is illustrated by Fig 2(d), which shows schematically two islands A and C separated by WL and typical dI/dV spectra in islands and WL between them. From the comparison of superconducting gaps in amorphous WL in the absence of Pb islands and their presence, it is clear that these islands greatly enhance superconducting correlations in WL due to the proximity effect in a substrate.

Figure 3 shows a dependence of the supercon-

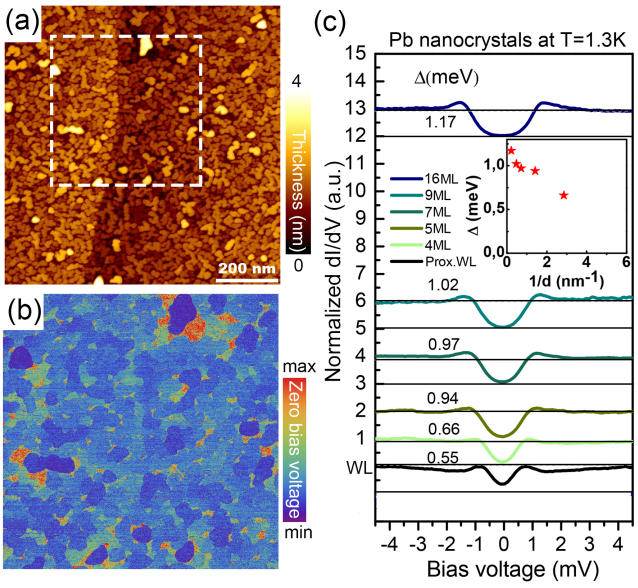

Figure 3: STM/STS maps acquired at 1.3 K: (a) – 800×800 nm^2 STM image of Pb islands on the surface of Bi_2Te_3 after 15 minute RT deposition of Pb; (b) – zero-bias conductance map of the rectangular area marked by the dashed line on (a); (c) – normalized dI/dV spectrum dependencies as a function of Pb islands thickness (ML), where the black line corresponds to proximised wetting layer. In addition, the insert depicts the behaviour of the Pb superconducting gap (Δ) as the inverse thickness of Pb islands varies.

ducting gap on Pb island thickness. Fig. 3(a) demonstrates the STM topography map and corresponds to many islands. Fig. 3(b) is the ZBC map of a rectangular area marked by the dashed line in Fig. 3(a). Fig. 3(c) shows spectra for islands of several thicknesses, while the inset demonstrates the decrease of a superconducting gap as island thickness decreases explicitly. The results are in a qualitative agreement with previous works[44,57,58]

Pb islands inducing superconducting correlations in the wetting layer since the wetting layer itself is a normal diffusive metal with a proximity gap fast decaying from the island edge, as it was reported in experiments where insulating Si substrates have been used.[44,46] In contrast, we observe a non-vanishing proximity gap in the wetting layer and attribute it to the proximity

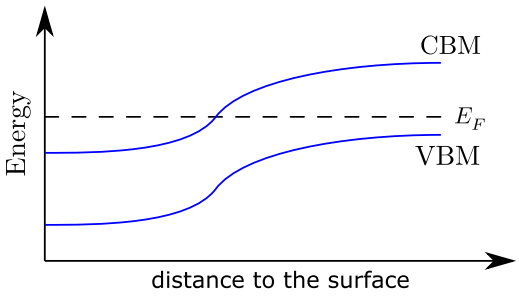

Figure 4: Schematic picture of the band bending near the surface of Bi_2Te_3.

effect induced by underneath surface states of Bi_2Te_3.

It is known that there are two different conductivity channels associated with the surface of a topological insulator Bi_2Te_3 (see, e.g., Ref.[59]). The channel of the first type is due to topologically protected gapless Dirac states. In contrast, the second type of channel is due to a more conventional two-dimensional electron gas of accumulation layer. The latter is quite common for Bi_2Te_3.[59] It can be induced by bulk band bending near the surface or by native defects and dangling bonds present on the surface.[59] In practice, it is not easy to distinguish between the two conductivity channels. In our system, the topological insulator is covered by the additional layer of Pb, and these two materials have different work functions, which are nearly 4.1 eV for Pb[60,61] and 5.3 eV for Bi_2Te_3.[62] Thus, the work function for Bi_2Te_3 is larger, and this is expected to result in the downward band bending at the Bi_2Te_3 surface. This phenomenon is schematically illustrated in Fig. 4. Fermi energy E_F is between valence band maximum (VBM) and conduction band minimum (CBM) far from the surface, but both of them are shifted downwards at the surface, so that E_F can reside above CBM. The additional downward band bending at the surface thus supports the formation of the electron gas of the accumulation layer. A similar band banding effect was described at[63] where Pb/InAs interface was studied.

These arguments are in full agreement with the results of DFT calculations, which are presented in Fig. 5. As shown in Fig. 5, the

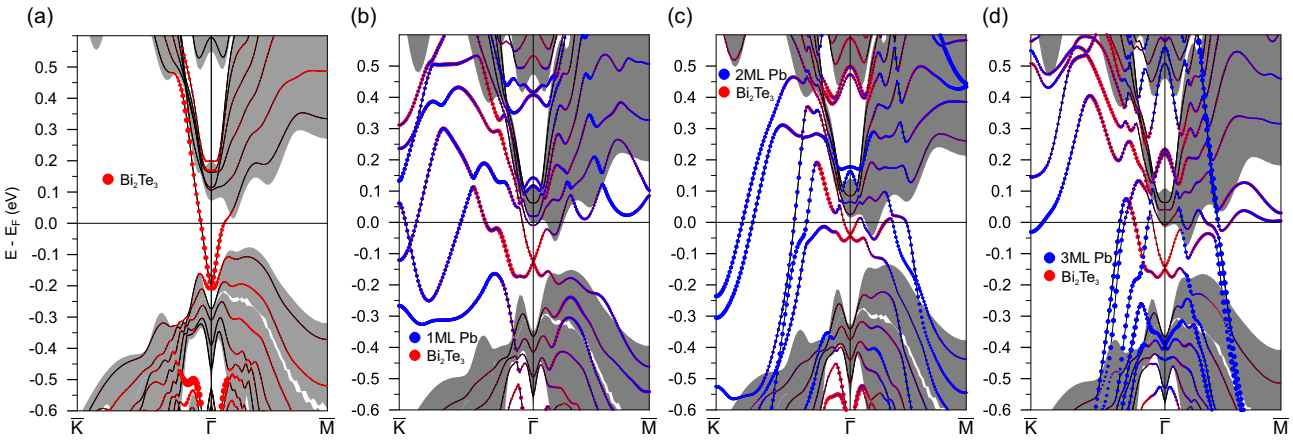

Figure 5: (a,b,c,d) Surface electronic structure of clean Bi_2Te_3 and with 1, 2 and 3 Pb monolayer films, respectively. Red and blue colours denote the states localized in the Bi_2Te_3 outer most quintuple layer and the Pb films, respectively. Grey background shows a projection of Bi_2Te_3 bulk bands onto (0001) surface

deposition of Pb monolayer film leads to the downward shift of the Bi_2Te_3 bulk continuum compared to pure Bi_2Te_3. Along with this, the Dirac point is displaced to the higher energy within the bulk bandgap, and such a displacement is more sizable in the case of two monolayers of Pb. According to our calculations, the work function for Bi_2Te_3 amounts to 5 eV what is in good agreement with other theoretical results.[64] Deposition of Pb monolayer films on the (0001) surface of Bi_2Te_3 leads to a significant decrease in the work function. Moreover, we found an oscillation of the work function values depending on the Pb film thickness: in one monolayer Pb the work function is equal to 3.3 eV, two monolayers Pb - 4.04 eV and three monolayers Pb - 3.65 eV. Note that these oscillations are typical for freestanding Pb monolayer films.[65] In any case, as expected, the work function of Pb/Bi_2Te_3 is lower than for pure Bi_2Te_3 (Fig.5(a)). The surface electronic structure strongly depends on the number of Pb monolayers. The precise mechanism of the superconducting proximity effect might depend on the fine structure of atoms arrangement at the interface. Moreover, the modification of electronic structure underneath the amorphous wetting layer must also be different from underneath the islands.

Thus, we expect that Pb islands placed on topological insulator Bi_2Te_3 induce superconducting correlations due to the proximity effect. The correlations can be associated with two conductivity channels, either by Dirac electrons or by the electrons of the accumulation layer formed due to the band bending. The two types of electronic surface states have approximately the same Fermi velocities,[66] which for Bi_2Te_3 are estimated as $v_F \sim 5 \cdot 10^5\ m/s$.[29,41] The expression, which allows us to estimate superconducting coherence length in both the Dirac and conventional two-dimensional electron gases, is

$$\xi = \frac{\hbar v_F}{\Delta_{TI}},$$

where $\Delta_{TI} \sim 1$ meV is the proximity induced superconducting gap in the topological insulator. We assumed that the contact between Pb and the topological insulator is highly transparent[20,67,68] that justifies our estimate for ξ, as follows from the solution of Bogoliubov-de Gennes equations,[69] so that gaps in Pb and at the surface are of the same order. Actually, this is exactly what we see in STM experiments – the superconducting gap at the wetting layer is approximately twice lower than in Pb islands. Since superconducting correlations at the wetting layer are induced from the underlying topological insulator surface, we may conclude that the gap under the wetting layer is not smaller. Thus, the coherence length at the topological

insulator surface is estimated to be as long as $\xi \sim 1\ \mu m$. Moreover, this length due to conductivity within the Dirac channel must be larger than the length due to the two-dimensional electron gas, since v_F for Dirac states is of the same order but still larger. Of course, this is an oversimplified picture. At the same time, the actual situation might be more subtle and, in particular, dependent on the details of the arrangement of Pb atoms at the interface. Our simple estimates follow that ξ, within any of the two channels, exceeds by one or two orders in magnitude typical distance between Pb islands. These proximity induced superconducting correlations cover the whole space between islands and, as a result, support the superconductivity in the wetting layer of Pb.

The additional evidence of the suggested mechanism comes from the comparison with the results of Refs.,[44,70–73] where similar Pb islands grown on Si substrate have been studied by STM. These studies revealed specific features in dI/dV spectra on top of the islands attributed to quantum-well states and the formation of two-dimensional bands. However, such features was not observed in our case, can bee linked to the islands' connection to the conducting substrate.

In summary, we demonstrated a self-organized Pb/Bi_2Te_3 structure and investigated the local conductance spatial distribution at the interface between superconducting Pb and bulk topological insulator. Pb forms islands grown on atomically clean surfaces of Bi_2Te_3 as well as an amorphous wetting layer between individual islands. An anomalously strong superconducting proximity effect between Bi_2Te_3 and wetting layer is revealed, attributed to superconducting correlations induced in topological insulator by Pb islands. We argued that there might be at least two conductivity channels associated with the surface of Bi_2Te_3, either due to Dirac electrons or the accumulation layer's normal electrons, formed by the downward band bending at the surface. DFT calculations indeed have shown that the presence of Pb monolayers at the surface of Bi_2Te_3 leads to the modification of surface electronic structure, which strongly depends on the number of layers. Thus, our results suggest that a detailed arrangement of Pb atoms at the surface of Bi_2Te_3 must be considered to describe induced superconductivity in this topological insulator adequately.

Methods. The experiments were performed in ultra-high vacuum (UHV, base pressure $<2\times10^{-10}$ mbar). Five nominal monolayers (ML) of Pb were deposited at room temperature at the deposition rate 1 Å/min onto in vacuum cleaved surface of Bi_2Te_3 single crystals. STM/STS measurements were performed at 1.3 K in the same UHV environment. Local tunneling conductance $dI(V,x,y)/dV$ spectra were obtained by the numerical derivative of the raw $I(V,x,y)$ data.

Electronic structure calculations were carried out within the density functional theory using the projector augmented-wave method[74,75] as implemented in the VASP.[76] To describe the exchange-correlation energy, we used the generalized gradient approximation (GGA) with the PBE functional.[77] In addition, the Hamiltonian contained scalar relativistic corrections, and the spin-orbit coupling was taken into account by the second variation method.[78] The film calculations presented in this work were performed using symmetric setups, so the upper and lower surfaces are identical. The work function values for the Pb films of 1,2 and 3 ML's on top of Bi_2Te_3 were calculated as the difference between energies of the vacuum and Fermi levels of the corresponding slabs. In the case of clean Bi_2Te_3, the value of the work function was estimated as the difference between energies of the vacuum level and valence band maximum of the slab.[79]

Acknowledgement Useful comments by R. S. Akzyanov and A. V. Rozhkov are acknowledged. The STM experiments were carried out with the support of the RSF-ANR (project No. 20-42-09033). T.V.M. acknowledges support from RSF within the research project No. 18-12-00169 [DFT calculations of the Bi_2Te_3 with Pb MLs]. Yu.E.L. acknowledge Program of Basic Research of HSE.

References

(1) Delagebeaudeuf, D.; Linh, N. Metal-(n) AlGaAs-GaAs two-dimensional electron gas FET. *IEEE Transactions on Electron Devices* **1982**, *29*, 955–960.

(2) Gao, Z.; Huang, X.; Li, P.; Wang, L.; Wei, L.; Zhang, W.; Guo, H. Reversible Resistance Switching of 2D Electron Gas at $LaAlO_3/SrTiO_3$ Heterointerface. *Advanced Materials Interfaces* **2018**, *5*, 1701565.

(3) Novoselov, K. S.; Geim, A. K.; Morozov, S. V.; Jiang, D.; Zhang, Y.; Dubonos, S. V.; Grigorieva, I. V.; Firsov, A. A. Electric Field Effect in Atomically Thin Carbon Films. *Science* **2004**, *306*, 666–669.

(4) Tresca, C.; Brun, C.; Bilgeri, T.; Menard, G.; Cherkez, V.; Federicci, R.; Longo, D.; Debontridder, F.; D'angelo, M.; Roditchev, D.; Profeta, G.; Calandra, M.; Cren, T. Chiral Spin Texture in the Charge-Density-Wave Phase of the Correlated Metallic Pb/Si(111) Monolayer. *Phys. Rev. Lett.* **2018**, *120*, 196402.

(5) Dubost, V.; Cren, T.; Vaju, C.; Cario, L.; Corraze, B.; Janod, E.; Debontridder, F.; Roditchev, D. Resistive Switching at the Nanoscale in the Mott Insulator Compound $GaTa_4Se_8$. *Nano Letters* **2013**, *13*, 3648–3653.

(6) Biscaras, J.; Bergeal, N.; Kushwaha, A.; Wolf, T.; Rastogi, A.; Budhani, R.; Lesueur, J. Two-dimensional superconductivity at a Mott insulator/band insulator interface $LaTiO_3/SrTiO_3$. *Nature Communications* **2010**, *1*, 89.

(7) Wan, Z.; Kazakov, A.; Manfra, M. J.; Pfeiffer, L. N.; West, K. W.; Rokhinson, L. P. Induced superconductivity in high-mobility two-dimensional electron gas in gallium arsenide heterostructures. *Nature Communications* **2015**, *6*, 7426.

(8) Nadj-Perge, S.; Drozdov, I. K.; Li, J.; Chen, H.; Jeon, S.; Seo, J.; MacDonald, A. H.; Bernevig, B. A.; Yazdani, A. Observation of Majorana fermions in ferromagnetic atomic chains on a superconductor. *Science* **2014**, *346*, 602–607.

(9) Menard, G. C.; Guissart, S.; Brun, C.; Leriche, R. T.; Trif, M.; Debontridder, F.; Demaille, D.; Roditchev, D.; Simon, P.; Cren, T. Two-dimensional topological superconductivity in Pb/Co/Si(111). *Nature Communications* **2017**, *8*, 2040.

(10) Ge, J.-F.; Liu, Z.-L.; Liu, C.; Gao, C.-L.; Qian, D.; Xue, Q.-K.; Liu, Y.; Jia, J.-F. Superconductivity above 100 K in single-layer FeSe films on doped $SrTiO_3$. *Nature Materials* **2015**, *14*, 285–289.

(11) Brun, C.; Cren, T.; Cherkez, V.; Debontridder, F.; Pons, S.; Fokin, D.; Tringides, M. C.; Bozhko, S.; Ioffe, L. B.; Altshuler, B. L.; Roditchev, D. Remarkable effects of disorder on superconductivity of single atomic layers of lead on silicon. *Nature Physics* **2015**, *10*, 444–450.

(12) de Gennes, P. G. Boundary Effects in Superconductors. *Rev. Mod. Phys.* **1964**, *36*, 225–237.

(13) Clarke, J. The Proximity Effect Between Superconducting and Normal Thin Films in Zero Field. *Journal de Physique Colloques* **1968**, *29*, C2–3–C2–16.

(14) le Sueur, H.; Joyez, P.; Pothier, H.; Urbina, C.; Esteve, D. Phase Controlled Superconducting Proximity Effect Probed by Tunneling Spectroscopy. *Phys. Rev. Lett.* **2008**, *100*, 197002.

(15) Karapetrov, G.; Fedor, J.; Iavarone, M.; Rosenmann, D.; Kwok, W. K. Direct Observation of Geometrical Phase Transitions in Mesoscopic Superconductors by Scanning Tunneling Microscopy. *Phys. Rev. Lett.* **2005**, *95*, 167002.

(16) Giazotto, F.; Peltonen, J. T.; Meschke, M.; Pekola, J. P. Superconducting quantum interference proximity transistor. *Nature Physics* **2010**, *6*, 254–259.

(17) Stolyarov, V. S.; Cren, T.; Debontridder, F.; Brun, C.; Veshchunov, I. S.; Skryabina, O. V.; Rusanov, A. Y.; Roditchev, D. Ex situ elaborated proximity mesoscopic structures for ultrahigh vacuum scanning tunneling spectroscopy. *Applied Physics Letters* **2014**, *104*, 172604.

(18) Stolyarov, V. S.; Cren, T.; Brun, C.; Golovchanskiy, I. A.; Skryabina, O. V.; Kasatonov, D. I.; Khapaev, M. M.; Kupriyanov, M. Y.; Golubov, A. A.; Roditchev, D. Expansion of a superconducting vortex core into a diffusive metal. *Nature Communications* **2018**, *9*, 2277.

(19) Skryabina, O. V.; Egorov, S. V.; Goncharova, A. S.; Klimenko, A. A.; Kozlov, S. N.; Ryazanov, V. V.; Bakurskiy, S. V.; Kupriyanov, M. Y.; Golubov, A. A.; Napolskii, K. S.; Stolyarov, V. S. Josephson coupling across a long single-crystalline Cu nanowire. *Applied Physics Letters* **2017**, *110*, 222605.

(20) Qu, F.; Yang, F.; Shen, J.; Ding, Y.; Chen, J.; Ji, Z.; Liu, G.; Fan, J.; Jing, X.; Yang, C.; Lu, L. Strong Superconducting Proximity Effect in Pb-Bi_2Te_3 Hybrid Structures. *Scientific Reports* **2012**, *2*, 339.

(21) Cleuziou, J.-P.; Wernsdorfer, W.; Bouchiat, V.; Ondarçuhu, T.; Monthioux, M. Carbon nanotube superconducting quantum interference device. *Nature Nanotechnology* **2012**, *1*, 53–59.

(22) Cherkez, V.; Mallet, P.; Le Quang, T.; Magaud, L.; Veuillen, J.-Y. Electronic properties of Pb islands on graphene: Consequences of a weak interface coupling from a combined STM and ab initio study. *Phys. Rev. B* **2018**, *98*, 195441.

(23) Stolyarov, V. S. et al. Josephson current mediated by ballistic topological states in $Bi_2Te_{2.3}Se_{0.7}$ single nanocrystals. *Communications Materials* **2020**, *1*, 38.

(24) Wang, Z.; Tang, C.; Sachs, R.; Barlas, Y.; Shi, J. Proximity-Induced Ferromagnetism in Graphene Revealed by the Anomalous Hall Effect. *Phys. Rev. Lett.* **2015**, *114*, 016603.

(25) Charpentier, S.; Galletti, L.; Kunakova, G.; Arpaia, R.; Song, Y.; Baghdadi, R.; Wang, S. M.; Kalaboukhov, A.; Olsson, E.; Tafuri, F.; Golubev, D.; Linder, J.; Bauch, T.; Lombardi, F. Induced unconventional superconductivity on the surface states of Bi_2Te_3 topological insulator. *Nature Communications* **2019**, *8*, 2017.

(26) Ren, X.-Y.; Kim, H.-J.; Yi, S.; Jia, Y.; Cho, J.-H. Spin-orbit coupling effects on the stability of two competing structures in Pb/Si(111) and Pb/Ge(111). *Phys. Rev. B* **2016**, *94*, 075436.

(27) Brand, C.; Muff, S.; Fanciulli, M.; Pfnür, H.; Tringides, M. C.; Dil, J. H.; Tegenkamp, C. Spin-resolved band structure of a densely packed Pb monolayer on Si(111). *Phys. Rev. B* **2017**, *96*, 035432.

(28) Kou, L.; Ma, Y.; Sun, Z.; Heine, T.; Chen, C. Two-Dimensional Topological Insulators: Progress and Prospects. *The Journal of Physical Chemistry Letters* **2017**, *8*, 1905–1919.

(29) Zhang, H.; Liu, C.-X.; Qi, X.-L.; Dai, X.; Fang, Z.; Zhang, S.-C. Topological insulators in Bi_2Se_3, Bi_2Te_3 and Sb_2Te_3 with a single Dirac cone on the surface. *Nature Physics* **2009**, *5*, 438–442.

(30) Hasan, M. Z.; Kane, C. L. Colloquium: Topological insulators. *Rev. Mod. Phys.* **2010**, *82*, 3045–3067.

(31) Qi, X.-L.; Zhang, S.-C. Topological insulators and superconductors. *Rev. Mod. Phys.* **2011**, *83*, 1057–1110.

(32) Fu, L.; Kane, C. L.; Mele, E. J. Topological Insulators in Three Dimensions. *Phys. Rev. Lett.* **2007**, *98*, 106803.

(33) Moore, J. E.; Balents, L. Topological invariants of time-reversal-invariant band structures. *Phys. Rev. B* **2007**, *75*, 121306.

(34) Hsieh, D. et al. A tunable topological insulator in the spin helical Dirac transport regime. *Nature* **2009**, *460*, 1101–1105.

(35) Si, N.; Yao, Q.; Jiang, Y.; Li, H.; Zhou, D.; Ji, Q.; Huang, H.; Li, H.; Niu, T. Recent Advances in Tin: From Two-Dimensional Quantum Spin Hall Insulator to Bulk Dirac Semimetal. *The Journal of Physical Chemistry Letters* **2020**, *11*, 1317–1329.

(36) Pi, S.-T.; Wang, H.; Kim, J.; Wu, R.; Wang, Y.-K.; Lu, C.-K. New Class of 3D Topological Insulator in Double Perovskite. *The Journal of Physical Chemistry Letters* **2017**, *8*, 332–339, PMID: 28026964.

(37) Tian, L.; Liu, Y.; Meng, W.; Zhang, X.; Dai, X.; Liu, G. Spin–Orbit Coupling-Determined Topological Phase: Topological Insulator and Quadratic Dirac Semimetals. *The Journal of Physical Chemistry Letters* **2020**, *11*, 10340–10347, PMID: 33232150.

(38) Xu, J.-P.; Wang, M.-X.; Liu, Z. L.; Ge, J.-F.; Yang, X.; Liu, C.; Xu, Z. A.; Guan, D.; Gao, C. L.; Qian, D.; Liu, Y.; Wang, Q.-H.; Zhang, F.-C.; Xue, Q.-K.; Jia, J.-F. Experimental Detection of a Majorana Mode in the core of a Magnetic Vortex inside a Topological Insulator-Superconductor $Bi_2Te_3/NbSe_2$ Heterostructure. *Phys. Rev. Lett.* **2015**, *114*, 017001.

(39) Liu, C.; Jia, J.-F. Creating Majorana fermions in topological insulators. *National Science Review* **2014**, *1*, 36–37.

(40) Yano, R.; Kudriashov, A.; Hirose, H. T.; Tsuda, T.; Kashiwaya, H.; Sasagawa, T.; Golubov, A. A.; Stolyarov, V. S.; Kashiwaya, S. Magnetic Gap of Fe-Doped BiSbTe2Se Bulk Single Crystals Detected by Tunneling Spectroscopy and Gate-Controlled Transports. *The Journal of Physical Chemistry Letters* **2021**, *12*, 4180–4186, PMID: 33900082.

(41) Beidenkopf, H.; Roushan, P.; Seo, J.; Gorman, L.; Drozdov, I.; Hor, Y. S.; Cava, R. J.; Yazdani, A. Spatial fluctuations of helical Dirac fermions on the surface of topological insulators. *Nature Physics* **2011**, *7*, 939–943.

(42) Sánchez-Barriga, J.; Battiato, M.; Krivenkov, M.; Golias, E.; Varykhalov, A.; Romualdi, A.; Yashina, L. V.; Minár, J.; Kornilov, O.; Ebert, H.; Held, K.; Braun, J. Subpicosecond spin dynamics of excited states in the topological insulator Bi_2Te_3. *Phys. Rev. B* **2017**, *95*, 125405.

(43) Xue, H.; Lv, W.; Wu, D.; Cai, J.; Ji, Z.; Zhang, Y.; Zeng, Z.; Jin, Q.; Zhang, Z. Temperature Dependence of Spin–Orbit Torques in Nearly Compensated $Tb_{21}Co_{79}$ Films by a Topological Insulator Sb_2Te_3. *The Journal of Physical Chemistry Letters* **2021**, *12*, 2394–2399, PMID: 33661010.

(44) Brun, C.; Hong, I.-P.; Patthey, F. m. c.; Sklyadneva, I. Y.; Heid, R.; Echenique, P. M.; Bohnen, K. P.; Chulkov, E. V.; Schneider, W.-D. Reduction of the Superconducting Gap of Ultrathin Pb Islands Grown on Si(111). *Phys. Rev. Lett.* **2009**, *102*, 207002.

(45) Cherkez, V.; Cuevas, J. C.; Brun, C.; Cren, T.; Ménard, G.; Debontridder, F.; Stolyarov, V. S.; Roditchev, D. Proximity Effect between Two Superconductors

Spatially Resolved by Scanning Tunneling Spectroscopy. *Phys. Rev. X* **2014**, *4*, 011033.

(46) Serrier-Garcia, L.; Cuevas, J. C.; Cren, T.; Brun, C.; Cherkez, V.; Debontridder, F.; Fokin, D.; Bergeret, F. S.; Roditchev, D. Scanning Tunneling Spectroscopy Study of the Proximity Effect in a Disordered Two-Dimensional Metal. *Phys. Rev. Lett.* **2013**, *110*, 157003.

(47) Vlaic, S.; Pons, S.; Zhang, T.; Assouline, A.; Zimmers, A.; David, C.; Rodary, G.; Girard, J.-C.; Roditchev, D.; Aubin, H. Superconducting parity effect across the Anderson limit. *Nature Communications* **2017**, *8*, 14549.

(48) Hwang, E. H.; Das Sarma, S. Limit to two-dimensional mobility in modulation-doped GaAs quantum structures: How to achieve a mobility of 100 million. *Phys. Rev. B* **2008**, *77*, 235437.

(49) Magnus, F.; Yates, K. A.; Clowes, S. K.; Miyoshi, Y.; Bugoslavsky, Y.; Cohen, L. F.; Aziz, A.; Burnell, G.; Blamire, M. G.; Josephs-Franks, P. W. Interface properties of PbInAs planar structures for Andreev spectroscopy. *Applied Physics Letters* **2008**, *92*, 012501.

(50) Vincent, T.; Vlaic, S.; Pons, S.; Zhang, T.; Aubin, H.; Stolyarov, V. S.; Ksenz, A. S.; Ionov, A. M.; Chekmazov, S. V.; Bozhko, S. I.; Roditchev, D. Strong coupling and periodic potential at the Pb/Sb(111) interface. *Phys. Rev. B* **2018**, *98*, 155440.

(51) Stolyarov, V. S.; Remizov, S. V.; Shapiro, D. S.; Pons, S.; Vlaic, S.; Aubin, H.; Baranov, D. S.; Brun, C.; Yashina, L. V.; Bozhko, S. I.; Cren, T.; Pogosov, W. V.; Roditchev, D. Double Fe-impurity charge state in the topological insulator Bi_2Se_3. *Applied Physics Letters* **2017**, *111*, 251601.

(52) Nikitin, A. Y.; Guinea, F.; García-Vidal, F. J.; Martín-Moreno, L. Edge and waveguide terahertz surface plasmon modes in graphene microribbons. *Phys. Rev. B* **2011**, *84*, 161407.

(53) Netsou, A.-M.; Muzychenko, D. A.; Dausy, H.; Chen, T.; Song, F.; Schouteden, K.; Van Bael, M. J.; Van Haesendonck, C. Identifying Native Point Defects in the Topological Insulator Bi_2Te_3. *ACS Nano* **2020**, *14*, 13172–13179.

(54) Stolyarov, V. S.; Sheina, V. A.; Khokhlov, D. A.; Vlaic, S.; Pons, S.; Aubin, H.; Akzyanov, R. S.; Vasenko, A. S.; Menshchikova, T. V.; Chulkov, E. V.; Golubov, A. A.; Cren, T.; Roditchev, D. Disorder-Promoted Splitting in Quasiparticle Interference at Nesting Vectors. *The Journal of Physical Chemistry Letters* **2021**, *12*, 3127–3134.

(55) Feng, R.; Conrad, E. H.; Tringides, M. C.; Kim, C.; Miceli, P. F. Wetting-layer transformation for Pb nanocrystals grown on Si(111). *Applied Physics Letters* **2004**, *85*, 3866–3868.

(56) Rollbühler, J.; Grabert, H. Coulomb Blockade of Tunneling between Disordered Conductors. *Phys. Rev. Lett.* **2001**, *87*, 126804.

(57) Eom, D.; Qin, S.; Chou, M.-Y.; Shih, C. K. Persistent Superconductivity in Ultrathin Pb Films: A Scanning Tunneling Spectroscopy Study. *Phys. Rev. Lett.* **2006**, *96*, 027005.

(58) Qin, S.; Kim, J.; Niu, Q.; Shih, C.-K. Superconductivity at the Two-Dimensional Limit. *Science* **2009**, *324*, 1314–1317.

(59) Suh, J.; Fu, D.; Liu, X.; Furdyna, J. K.; Yu, K. M.; Walukiewicz, W.; Wu, J. Fermi-level stabilization in the topological insulators Bi_2Se_3 and Bi_2Te_3: Origin of the surface electron gas. *Phys. Rev. B* **2014**, *89*, 115307.

(60) Qi, Y.; Ma, X.; Jiang, P.; Ji, S.; Fu, Y.; Jia, J.-F.; Xue, Q.-K.; Zhang, S. B. Atomic-layer-resolved local work functions

of Pb thin films and their dependence on quantum well states. *Applied Physics Letters* **2007**, *90*, 013109.

(61) Aladyshkin, A. Y. Quantum-well and modified image-potential states in thin Pb(111) films: an estimate for the local work function. *Journal of Physics: Condensed Matter* **2020**, *32*, 435001.

(62) Lee, E.; Ko, J.; Kim, J.-Y.; Seo, W.-S.; Choi, S.-M.; Lee, K. H.; Shim, W.; Lee, W. Enhanced thermoelectric properties of Au nanodot-included Bi2Te3 nanotube composites. *Journal of Materials Chemistry C* **2016**, *4*, 1313–1319.

(63) Zhang, T.; Vlaic, S.; Pons, S.; Assouline, A.; Zimmers, A.; Roditchev, D.; Aubin, H.; Allan, G.; Delerue, C.; David, C.; Rodary, G.; Girard, J.-C. Quantum confinement effects in Pb nanocrystals grown on InAs. *Phys. Rev. B* **2018**, *97*, 214514.

(64) Ryu, B. Work function of bismuth telluride: First-principles approach. *Journal of the Korean Physical Society* **2018**, *72*, 122–128.

(65) Li, C.; Chen, W.; Li, M.; Sun, Q.; Jia, Y. Thickness dependent of phase shift between surface energy and work function in Pb ultrathin films. *New Journal of Physics* **2015**, *17*, 053006.

(66) Chen, C. et al. Robustness of topological order and formation of quantum well states in topological insulators exposed to ambient environment. *Proceedings of the National Academy of Sciences* **2012**, *109*, 3694–3698.

(67) Stanescu, T. D.; Sau, J. D.; Lutchyn, R. M.; Das Sarma, S. Proximity effect at the superconductor–topological insulator interface. *Phys. Rev. B* **2010**, *81*, 241310.

(68) Zhang, Y.; Huang, J.; Zhang, C.; Wang, P.; Wang, Z.; Wang, T.; Xing, Z.; Xing, D. Y. Proximity-effect-induced superconductivity in $Bi_2Te_3/FeSe_{0.5}Te_{0.5}$ thin-film heterostructures with different interface conditions. *Phys. Rev. B* **2020**, *102*, 064503.

(69) Rakhmanov, A. L.; Rozhkov, A. V.; Nori, F. Majorana fermions in pinned vortices. *Phys. Rev. B* **2011**, *84*, 075141.

(70) Hong, I.-P.; Brun, C.; Patthey, F.; Sklyadneva, I. Y.; Zubizarreta, X.; Heid, R.; Silkin, V. M.; Echenique, P. M.; Bohnen, K. P.; Chulkov, E. V.; Schneider, W.-D. Decay mechanisms of excited electrons in quantum-well states of ultrathin Pb islands grown on Si(111): Scanning tunneling spectroscopy and theory. *Phys. Rev. B* **2009**, *80*, 081409.

(71) Ustavshchikov, S. S.; Putilov, A. V.; Aladyshkin, A. Y. Tunneling interferometry and measurement of the thickness of ultrathin metallic Pb(111) films. *JETP Letters* **2018**, *106*, 491–497.

(72) Altfeder, I. B.; Matveev, K. A.; Chen, D. M. Electron Fringes on a Quantum Wedge. *Phys. Rev. Lett.* **1997**, *78*, 2815–2818.

(73) Su, W. B.; Chang, S. H.; Jian, W. B.; Chang, C. S.; Chen, L. J.; Tsong, T. T. Correlation between Quantized Electronic States and Oscillatory Thickness Relaxations of 2D Pb Islands on Si(111)-(7×7) Surfaces. *Phys. Rev. Lett.* **2001**, *86*, 5116–5119.

(74) Blöchl, P. E. Projector augmented-wave method. *Phys. Rev. B* **1994**, *50*, 17953–17979.

(75) Kresse, G.; Joubert, D. From ultrasoft pseudopotentials to the projector augmented-wave method. *Phys. Rev. B* **1999**, *59*, 1758–1775.

(76) Kresse, G.; Furthmüller, J. Efficiency of ab-initio total energy calculations for metals and semiconductors using a plane-wave basis set. *Computational Materials Science* **1996**, *6*, 15–50.

(77) Perdew, J. P.; Burke, K.; Ernzerhof, M. Generalized Gradient Approximation Made Simple. *Phys. Rev. Lett.* **1996**, *77*, 3865–3868.

(78) Koelling, D. D.; Harmon, B. N. A technique for relativistic spin-polarised calculations. *Journal of Physics C: Solid State Physics* **1977**, *10*, 3107–3114.

(79) He, C. Work function of (001) and (00-1) surface of α-Fe2O3. *Modern Physics Letters B* **2018**, *32*, 1850188.